# Experimental Realization of Quantum Illumination

E. D. Lopaeva,[1,2] I. Ruo Berchera,[1] I. P. Degiovanni,[1] S. Olivares,[3,4,5] G. Brida,[1] and M. Genovese[1]

[1]*INRIM, Strada delle Cacce 91, I-10135 Torino, Italy*
[2]*Dipartimento di Fisica, Politecnico di Torino, I-10129 Torino, Italy*
[3]*Dipartimento di Fisica, Università degli Studi di Milano, I-20133 Milano, Italy*
[4]*Dipartimento di Fisica, Università degli Studi di Trieste, I-34151 Trieste, Italy*
[5]*CNISM UdR Milano Statale, I-20133 Milano, Italy*
(Received 21 January 2013; published 10 April 2013)

We present the first experimental realization of the quantum illumination protocol proposed by Lloyd [Science **321**, 1463 (2008)] and S. Tan *et al.* [Phys. Rev. Lett. **101**, 253601 (2008)], achieved in a simple feasible experimental scheme based on photon-number correlations. A main achievement of our result is the demonstration of a strong robustness of the quantum protocol to noise and losses that challenges some widespread wisdom about quantum technologies.

The properties of quantum states have disclosed the possibility of realizing tasks beyond classical limits, originating a field collectively christened quantum technology [1–7]. Among them, quantum metrology and imaging aim to improve the sensitivity and/or resolution of measurements exploiting nonclassical features, in particular, nonclassical correlations [8–12]. However, in most of the realistic scenarios, losses and noise are known to nullify the advantage of adopting quantum strategies [13]. Here, we present the first experimental realization of a quantum enhanced scheme [14,15], designed to target detection in a noisy environment, preserving a strong advantage over the classical counterparts even in presence of large amounts of noise and losses. This work, inspired by theoretical ideas elaborated in Refs. [14–17] (see also Ref. [18]), has been implemented exploiting only photon-number correlations in twin beams and, for its accessibility, it can find widespread use. Even more important, it paves the way to the real application of quantum technologies by challenging the common belief that they are limited by their fragility to noise and losses.

Our scheme for target detection is inspired by the ''quantum illumination'' (QI) idea [14,15], where the correlation between two beams of a bipartite nonclassical state of light is used to detect the target hidden in a noisy thermal background, which is partially reflecting one of the beams. In Refs. [15,16] it was shown that for QI realized by twin beams, like the ones produced by parametric down-conversion, there exists, in principle, an optimal reception strategy offering a significant performance gain with respect to any classical strategy. Unfortunately, this quantum optimal receiver is not yet devised, and even the theoretical proposal of a suboptimal quantum receiver [19] was very challenging from an experimental point of view, and has not been realized yet.

Our aim is to lead the QI idea to an experimental demonstration in a realistic scenario. Therefore, in our realization we consider a realistic *a priori* unknown background, and a reception strategy based on photon-counting detection and second-order correlation measurements. We demonstrate that the quantum protocol performs astonishingly better than its classical counterpart based on classically correlated light at any background noise level. More in detail, we compare quantum illumination, specifically twin beams (TWB), with classical illumination (CI) based on correlated thermal beams, that turns out to be the best possible classical strategy in this detection framework.

On the one hand, our approach, based on a specific and affordable detection strategy in the context of the current technology, cannot aim to achieve the optimal target-detection bounds of Ref. [15], based on the quantum Chernoff bound [20–22]. On the other hand, it maintains most of the appealing features of the original idea, like a huge quantum enhancement and a robustness against noise, paving the way to future practical application because of the accessible measurement technique. Our study also provides a significant example of an ancilla-assisted quantum protocol, besides the few previous realizations, e.g., Refs. [11,23–25].

In our setup (see Fig. 1) parametric down-conversion (PDC) is exploited to generate two correlated light emissions with an average number of PDC photons per spatiotemporal mode, $\mu = 0.075$, that are then addressed to a high quantum efficiency CCD camera (See Supplemental Material, Sec. I [26]). In the QI protocol [Fig. 1(a)], one beam is directly detected, while a target object [a 50:50 beam splitter (BS)] is posed on the path of the other one, where it is superimposed with a thermal background produced by scattering a laser beam on an Arecchi's rotating ground glass. When the object is removed, only the background reaches the detector. The CCD camera detects, on different areas, both the optical paths. In the CI protocol [Fig. 1(b)], the TWB are substituted with classical correlated beams obtained by splitting a single arm of PDC,
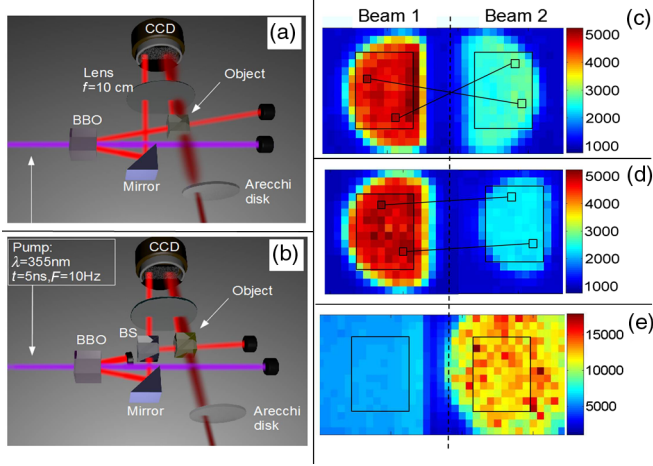
FIG. 1 (color online). Experimental setup. (a) Quantum illumination: after the beta-barium borate (BBO) crystal, where TWB are generated, one of them (the "ancilla") is reflected toward the detection system. The correlated beam is partially detected, together with the thermal field from the Arecchi's disk, when the object (actually a beam splitter) is present, otherwise it is lost (not shown). A low-pass filter (95% of the transmission at 710 nm) and a UV-reflecting mirror (not shown) are used to minimize the background noise while maintaining low losses. The lens, placed at the focal length from the crystal and the CCD camera, realizes the Fourier transform of the field at the output face of the crystal. (b) Classical illumination: one beam from PDC is stopped and the other one is split at a BS for generating correlated multithermal beams. The power of the pump is adjusted to obtain the same energy of the TWB. (c) Detected TWB, in the presence of the object, without thermal background. The region of interest is selected by an interference filter centered around the degeneracy wavelength (710 nm) and a bandwidth of 10 nm. After selection, the filter is removed. (d) Detected field for split thermal beams in the presence of the object, without thermal noise. (e) A typical frame used for the measurement where a strong thermal background has been added on the object branch. The color (intensity) scales on the right correspond to the number of photons per pixel.

which is a multithermal beam, and by adjusting the pump intensity to ensure the same intensity, time, and spatial coherence properties for the quantum and the classical sources.

We measured the correlation in the photon numbers $N_1$ and $N_2$ detected by pairs of pixels intercepting correlated modes of beams "1" and "2," respectively [Figs. 1(c)–1(e), [27,28]]. With our experimental setup, this correlation can be evaluated with a single image by averaging over all the $N_{pix}$ pixels pairs. Although the use of a spatial statistic is not strictly necessary, it is practically effective and allows us to reduce the measurement time (less images needed) [29].

In order to quantify the quantum resources exploited by our QI strategy, we introduce a suitable nonclassicality parameter: the generalized Cauchy-Schwarz parameter $\varepsilon = \langle :\delta N_1 \delta N_2: \rangle / \sqrt{\langle :\delta^2 N_1: \rangle \langle :\delta^2 N_2: \rangle}$, where $\langle :: \rangle$ is the normally ordered quantum expectation value and
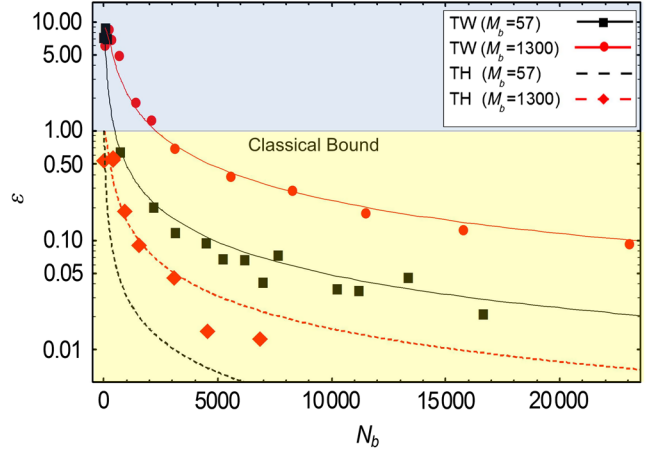


FIG. 2 (color online). Generalized Cauchy-Schwarz parameter $\varepsilon$ in the case of twin beams, $\varepsilon^{TW}$, and of the correlated thermal beams, $\varepsilon^{TH}$, as a function of the average number of background photons $\langle N_b \rangle$ for a number of background modes $M_b = 57$ (black squares series) and $M_b = 1300$ (red circles and diamonds). The lines represent the theoretical prediction at $\mu = 0.075$ (the last estimated independently).

$\delta^2 N_i = (N_i - \langle N_i \rangle)^2$ is the fluctuation of the photon number $N_i$, $i = 1, 2$. This parameter is interesting since it does not depend on the losses and it quantifies nonclassicality: $\varepsilon \le 1$ for the classical state of light (with a positive Glauber-Sudarshan $P$ function), while a quantum state with a negative or singular $P$ function can violate this bound [30]. In Fig. 2 we report the measured $\varepsilon$ and the theoretical prediction. One observes that for TWB $\varepsilon^{QI}$ is actually in the quantum regime [$\varepsilon^{QI} > 1$] for small values of the thermal background $\langle N_b \rangle$; in absence of it ($\langle N_b \rangle = 0$) we obtain $\varepsilon_0^{QI} \simeq 10$. As soon as the contribution of the background to the fluctuation of $N_2$ becomes dominant, $\varepsilon^{QI}$ decreases quite fast, well below the classical threshold. As expected, for thermal beams $\varepsilon^{CI}$ is always in the classical regime, and it is equal to one for $\langle N_b \rangle = 0$.

We consider an *a priori* unknown background, meaning that it is impossible to establish a reference threshold of photocounts (usually the mean value of the background) to be compared with the possible additional mean photocounts coming from the reflected probe beam (if the target is present). Therefore, the estimation of the first order (mean values) of the photocounts' distribution, typical of other protocols (e.g., Refs. [9,11,12]), is here not informative regarding the presence or absence of the object. We underline that this unknown-background hypothesis accounts for a "realistic" scenario where background properties can randomly change and drift with time and space.

For this reason we propose to discriminate the presence or absence of the object by distinguishing between the two corresponding values of the covariance $\Delta_{1,2}$, evaluated experimentally as

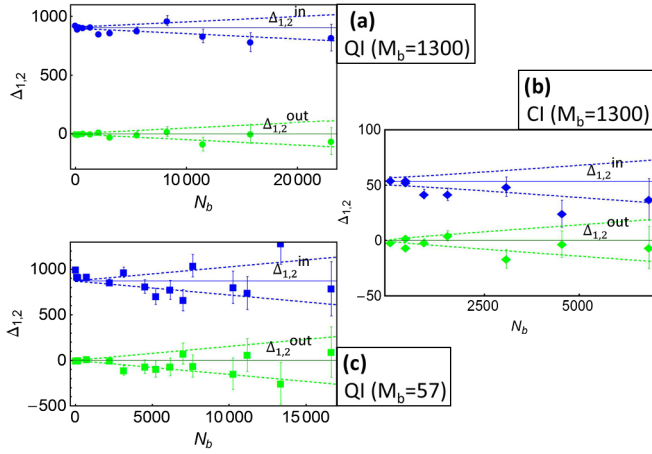$$\Delta_{1,2} = E[N_1 N_2] - E[N_1]E[N_2]. \tag{1}$$

FIG. 3 (color online). Covariance in the presence, $\Delta_{1,2}^{\text{in}}$ (dark blue), or absence, $\Delta_{1,2}^{\text{out}}$ (light green), of the target. Panels (a) and (b) refer to QI and CI, respectively, for the same number of background modes $M_b = 1300$; panel (c) refers to QI with a lower number of modes, $M_b = 57$. Uncertainty bars represent the effect of the background noise on the covariance estimation (obtained averaging over the $N_{\text{img}} = 2000$, 6000, and 4000 images in the graphs from the top to bottom, respectively). Horizontal lines are the theoretical values $\langle \Delta_{1,2}^{\text{in/out}} \rangle$, while the dashed lines are the uncertainty interval evaluated theoretically as $\langle \delta^2 \Delta_{1,2}^{\text{in/out}} \rangle / \sqrt{N_{\text{img}}}$.

$E[X] = \frac{1}{\mathcal{K}} \sum_{k=1}^{\mathcal{K}} X^{(k)}$ represents the average over the set of $\mathcal{K}$ realizations that, in our experiment, correspond to the number $\mathcal{K} = N_{\text{pix}}$ correlated pixels pairs. The signal-to-noise ratio can be defined as the ratio of the mean "contrast" to its standard deviation (mean fluctuation):

$$f_{\text{SNR}} \equiv \frac{|\langle \Delta_{1,2}^{\text{in}} - \Delta_{1,2}^{\text{out}} \rangle|}{\sqrt{\langle \delta^2 (\Delta_{1,2}^{\text{in}}) \rangle + \langle \delta^2 (\Delta_{1,2}^{\text{out}}) \rangle}}, \qquad (2)$$

where "in" and "out" refer to the presence and absence of the object.

For $\mathcal{K} \gg 1$, the contrast at the numerator of Eq. (2) corresponds to the quantum expected value of the covariance, i.e., $\langle \Delta_{1,2}^{\text{in}} \rangle \simeq \langle \delta N_1 \delta N_2 \rangle$, where obviously $\langle \Delta_{1,2}^{\text{out}} \rangle = 0$. For a generic prominent background with a mean square fluctuation $\langle \delta^2 N_b \rangle$, the "noise" at the denominator depends only on the local statistical properties of beam 1 and of the uncorrelated background, i.e., $\langle \delta^2 \Delta_{1,2} \rangle \simeq \langle \delta^2 N_1 \rangle \langle \delta^2 N_b \rangle$ (see Supplemental Material, Sec. II-a [26]). This is shown in Fig. 3, where the estimated covariance of Eq. (1) is plotted versus the intensity of the thermal background used in our experiment. As expected, the average value of covariance does not depend on the quantity of the environmental noise, while the uncertainty bars do.

While the signal-to-noise ratio unavoidably decreases with the added noise for both QI and CI, the quantum enhancement parameter $[R = f_{\text{SNR}}^{\text{QI}} / f_{\text{SNR}}^{\text{CI}}]$ in the presence

of the dominant background and equal local resources becomes

$$R \approx \langle \delta N_1 \delta N_2 \rangle_{\text{QI}} / \langle \delta N_1 \delta N_2 \rangle_{\text{CI}}. \qquad (3)$$

Being $R$ expressed as a ratio of covariances, it is remarkably independent on the amount of losses, noise, and reflectivity of the object.

According to Eq. (3), the enhancement is lower bounded by the amount of violation of the Cauchy-Schwarz inequality for the quantum state considered in the absence of the background, i.e., $R \simeq \varepsilon^{\text{QI}} / \varepsilon^{\text{CI}} \geq \varepsilon_0^{\text{QI}}$. The equality holds for classical states saturating the classical bound, $\varepsilon_0^{\text{CI}} = 1$ (see Supplemental Material, Sec. B [26]).

In particular, in our experiment we compared the performance of TWB with a classically correlated state with $\varepsilon_0^{\text{CI}} = 1$ (hence representing the best possible strategy), i.e., with a split thermal beams presenting the same local behavior of the TWB. In this case, the enhancement can be explicitly calculated obtaining $R \simeq (1 + \mu)/\mu$; hence, the quantum strategy performs orders of magnitude better than the classical analogous strategy when $\mu \ll 1$, namely, when a low intensity probe is used.

Incidentally, since covariance is always zero (i.e., $\varepsilon = 0$) when using split coherent beams, they do not provide a valuable alternative in the situation considered here, i.e., when first order momenta are not informative due to an unknown fluctuating background.

In Fig. 4, the theoretical prediction for $f_{\text{SNR}}/\sqrt{\mathcal{K}}$ is compared with the experimental data. In perfect agreement
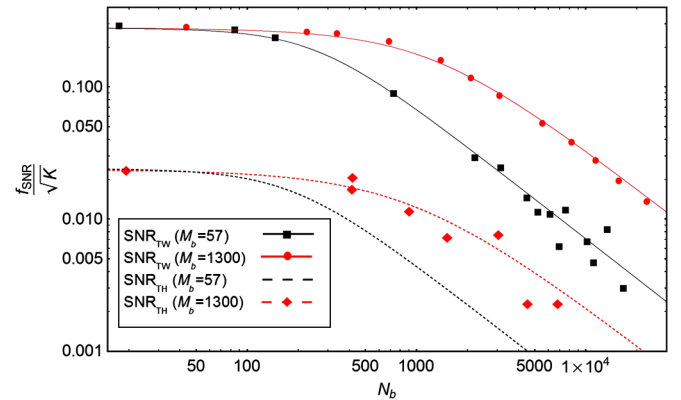


FIG. 4 (color online). Signal-to-noise ratio (SNR) versus the number of background photons $\langle N_b \rangle$ normalized by the square root of the number of realization. The red (black) markers refer to $M_b = 1300$ ($M_b = 57$) and the solid (dashed) theoretical curve corresponds to quantum (classical) illuminating beams. The estimation of quantum mean values of Eq. (2) is obtained by performing averages of $\Delta_{1,2}^{\text{in/out}}$ over a set of $N_{\text{img}}$ acquired images ($N_{\text{img}} = 2000$, 4000, and 6000 for twin beams at $M_b = 1300$, $M_b = 57$, and thermal beams at $M_b = 1300$, respectively). The lowest curve of the classical protocol has not been compared with the experimental data because the SNR is so low that a very large number of images (out of the possibility of the actual setup) is required to get reliable points.
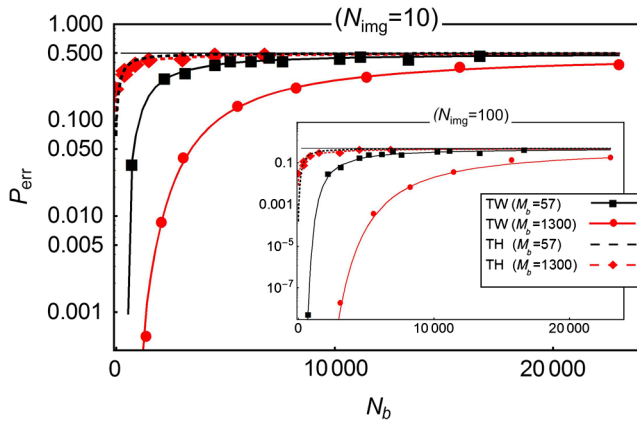
FIG. 5 (color online). Error probability $P_{\mathrm{err}}$ of the target detection versus the total number of photons of the thermal background $N_b$ evaluated with $N_{\mathrm{img}} = 10$ ($N_{\mathrm{img}} = 100$ in the inset). The black squares and red circles are the data for QI with $M_b = 57$ and $M_b = 1300$, respectively, while red diamonds refer to the data for the CI with $M_b = 1300$. The curves are the corresponding theoretical predictions.

with theory, the quantum enhancement is almost constant ($R \gtrsim 10$) regardless the value of $\langle N_b \rangle$. Therefore, the measurement time, i.e., the number of repetitions $N_{\mathrm{img}}$ needed for discriminating the presence or absence of the target, is dramatically reduced in QI (for instance, to achieve $f_{\mathrm{SNR}} = 1$, $N_{\mathrm{img}}$ is almost 100 times smaller when quantum correlations are exploited).

Another figure of merit that highlights the superiority of the quantum strategy versus the classical one is the the error probability in the discrimination of the presence or absence of the target ($P_{\mathrm{err}}$). In Fig. 5 we report $P_{\mathrm{err}}$ versus the number of photons of the thermal background $\langle N_b \rangle$. $P_{\mathrm{err}}$ is estimated by fixing the threshold value of the covariance that minimizes the error probability itself. Figure 5 shows a remarkable agreement between the theoretical predictions (lines) and the experimental data (symbols), both for QI and CI strategies. $P_{\mathrm{err}}$ of QI is several orders of magnitude below the CI one and, in terms of background photons, the same value of the error probability is reached for a value of $N_b$ at least 10 times smaller than in the QI case.

In conclusion, we demonstrated experimentally quantum enhancement in detecting a target in a thermal radiation background. Our system shows quantum correlation [$\varepsilon_0^{\mathrm{QI}} \simeq 10$] even in presence of losses introduced by a partially reflective target. Remarkably, even after the transition to the classical regime [$\varepsilon^{\mathrm{QI}} \ll 1$] due to the presence of the background ($\langle N_b \rangle \gg 1$), the scheme preserves the same strong advantage with respect to the best classical counterpart based on classically correlated thermal beams. Furthermore, the results are general and do not depend on the specific properties of the background used in the experiment.

In paradigmatic quantum enhanced schemes, often based on the experimental estimation of the first momenta

of the photon-number distribution, such as quantum imaging protocol [11], the detection of small beam displacement [9] and phase estimation by interferometry [12], it is well known that losses and noise rapidly decrease the advantage of using quantum light [13,31]. This is enforced inside the generic scientific community by the common belief that the advantages of entangled and quantum state are hardly applicable in a real context, and they will remain limited to experiments in highly controlled laboratories, and/or to mere academic discussions. Our work breaks this belief by showing orders of magnitude improvements compared to CI protocol, independent of the amount of noise and losses using devices available nowadays. In summary, we believe that the photon-counting based QI protocol, for its robustness to noise and losses, has a huge potentiality to promote the usage of quantum correlated light in real environments.

[1] D. Bouwmeester, J.-W. Pan, K. Mattle, M. Eibl, H. Weinfurter, and A. Zeilinger, Nature (London) **390**, 575 (1997).
[2] D. Boschi, S. Branca, F. De Martini, L. Hardy, and S. Popescu, Phys. Rev. Lett. **80**, 1121 (1998).
[3] J. L. O'Brien, Science **318**, 1567 (2007).
[4] X. Yao et al., Nature (London) **482**, 489 (2012).
[5] T. Yamamoto, M. Koashi, S. K. Özdemir, and N. Imoto, Nature (London) **421**, 343 (2003).
[6] J. W. Pan, C. Simon, C. Brukner, and A. Zeilinger, Nature (London) **410**, 1067 (2001).
[7] J. W. Pan, S. Gasparoni, R. Ursin, G. Weihs, and A. Zeilinger, Nature (London) **423**, 417 (2003).
[8] Quantum Imaging, edited by M. I. Kolobov (Springer, New York, 2007).
[9] N. Treps et al., Science **301**, 940 (2003).
[10] V. Boyer, A. M. Marino, R. C. Pooser, and P. D. Lett, Science **321**, 544 (2008).
[11] G. Brida, M. Genovese, and I. Ruo Berchera, Nat. Photonics **4**, 227 (2010).
[12] V. Giovannetti, S. Lloyd, and L. Maccone, Nat. Photonics **5**, 222 (2011).
[13] N. Thomas-Peter, B. J. Smith, A. Datta, L. Zhang, U. Dorner, and I. A. Walmsley, Phys. Rev. Lett. **107**, 113603 (2011).
[14] S. Lloyd, Science **321**, 1463 (2008).
[15] S. Tan, B. Erkmen, V. Giovannetti, S. Guha, S. Lloyd, L. Maccone, S. Pirandola, and J. Shapiro, Phys. Rev. Lett. **101**, 253601 (2008).
[16] J. H. Shapiro and S. Lloyd, New J. Phys. **11**, 063045 (2009).

[17] S. Guha and B. I. Erkmen, Phys. Rev. A **80**, 052310 (2009).

[18] M. F. Sacchi, Phys. Rev. A **71**, 062340 (2005); **72**, 014305 (2005).

[19] J. H. Shapiro, Phys. Rev. A **80**, 022320 (2009).

[20] K. M. R. Audenaert, Ll. Masanes, A. Acin, and F. Verstraete, Phys. Rev. Lett. **98**, 160501 (2007).

[21] S. Pirandola and S. Lloyd, Phys. Rev. A **78**, 012331 (2008).

[22] J. Calsamiglia, R. Muñoz-Tapia, Ll. Masanes, A. Acin, and E. Bagan, Phys. Rev. A **77**, 032311 (2008).

[23] G. Brida, L. Ciavarella, I. P. Degiovanni, M. Genovese, A. Migdall, M. G. Mingolla, M. G. A. Paris, F. Piacentini, and S. V. Polyakov, Phys. Rev. Lett. **108**, 253601 (2012).

[24] H. Takahashi, K. Wakui, S. Suzuki, M. Takeoka, K. Hayasaka, A. Furusawa, and M. Sasaki, Phys. Rev. Lett. **101**, 233605 (2008).

[25] J. B. Altepeter, D. Branning, E. Jeffrey, T. Wei, P. Kwiat, R. Thew, J. O'Brien, M. Nielsen, and A. White, Phys. Rev. Lett. **90**, 193601 (2003).

[26] See Supplemental Material at http://link.aps.org/supplemental/10.1103/PhysRevLett.110.153603 for more detailed descriptions and calculations.

[27] E. Brambilla, A. Gatti, M. Bache, and L. A. Lugiato, Phys. Rev. A **69**, 023802 (2004).

[28] G. Brida, M. Genovese, A. Meda, and I. Ruo Berchera, Phys. Rev. A **83**, 033811 (2011); G. Brida, L. Caspani, A. Gatti, M. Genovese, A. Meda, and I. Ruo-Berchera, Phys. Rev. Lett. **102**, 213602 (2009).

[29] G. Brida, I. P. Degiovanni, M. Genovese, M. L. Rastello, and I. Ruo Berchera, Opt. Express **18**, 20 572 (2010).

[30] P. Sekatski, N. Sangouard, F. Bussières, C. Clausen, N. Gisin, and H. Zbinden, J. Phys. B **45**, 124016 (2012).

[31] T. Iskhakov, M. V. Chekhova, and G. Leuchs, Phys. Rev. Lett. **102**, 183602 (2009).